# CHAOTIC DYNAMICS OF A NONLINEAR ELECTRONIC CONVERTER

E. CAMPOS-CANTÓN* , J.S. MURGUÍA* , H.C. ROSU‡

* *Departamento de Físico Matemáticas*
*Universidad Autónoma de San Luis Potosí, 78000, San Luis Potosí, SLP, México*
*ecamp@uaslp.mx, ondeleto@uaslp.mx*
‡ *Potosinian Institute of Science and Technology,*
*Apartado Postal 3-74 Tangamanga, 78231 San Luis Potosí, Mexico*
*hcr@ipicyt.edu.mx*

The nonlinear electronic converter used by Rulkov and collaborators [N.F. Rulkov *et al.* Phys. Rev. E **64**, 016217 (2001)], which is the core of their chaotic oscillator, is modeled and simulated numerically by means of an appropriate *direct* relationship between the experimental values of the electronic components of the system and the mathematical model. This relationship allows us to analyze the chaotic behavior of the model in terms of a particular bifurcation parameter $k$. Varying the parameter $k$, quantitative results of the dynamics of the numerical system are presented, which are found to be in good agreement with the experimental measurements that we performed as well. Moreover, we show that this nonlinear converter belongs to a class of 3-D systems that can be mapped to the unfolded Chua's circuit. We also report a wavelet transform analysis of the experimental and numerical chaotic time series data of this chaotic system. The wavelet analysis provides us with information on such systems in terms of the concentration of energy which is the standard electromagnetic interpretation of the $L^2$ norm of a given signal.

*Keywords:* Bifurcation analysis; chaotic time series; wavelet transform.

## 1. Introduction

The employment of electronic circuits that display various forms of nonlinear behavior is encountered in many physical, engineering, biological and other systems. In general, nonlinear circuit elements are in usage in electronic circuits with chaotic behavior. For instance Chua's electronic circuit employs a nonlinear negative resistance [Chua *et al.*, 1992], the Rössler electronic circuit proposed in [Carroll, 1995] also includes a nonlinear element in order to generate chaos. In these cases, the diode is the device that produces the nonlinearity. In the same spirit to Chua's circuit, Sprott [Kiers *et al.*, 2004, Sprott & Linz, 2000, Sprott, 2000] has described simple nonlinear electrical circuits to model continuous time flows. These circuits correspond to simple third-order differential equations with a particular nonlinear function and contain only simple electronic components such as resistors, capacitors, diodes, and operational amplifiers. In order to study chaos synchronization experimentally, some authors [Carroll, 1995, Chua *et al.*, 1992, Rulkov, 1996, Rulkov & Sushchick, 1997] have employed chaotic circuits, where again a nonlinear part of them is the core of the chaotic behavior. Rulkov [Rulkov, 1996, Rulkov & Sushchick, 1997] devised the nonlinear circuit part using an unspecified nonlinear amplifier to produce a particular form of the nonlinear input-output characteristics function $f(x)$. In the numerical simulation of this nonlinear circuit, in [Abarbanel *et al.*, 1993] and [Rulkov & Sushchick, 1997], empirical functions $f(x)$ have been used to model the nonlinear circuit. However, the parameters of this function do not have any relationship with the values of the electronic components of the nonlinear circuit.

In this paper we overcome this ambiguity by presenting a model of the nonlinear function with a direct relationship with the electric components of the nonlinear circuit and we study experimentally and

numerically the behavior of the chaotic circuit used by Rulkov [Rulkov, 1996, Rulkov & Sushchick, 1997, Rulkov *et al.*, 2001]. With the new form of $f(x)$ we perform a bifurcation analysis and a time chaotic series analysis by means of the wavelet transform. These procedures will allow us to quantify in more precise terms the behavior of this chaotic circuit.

The paper is organized in the following way. In Section 2, we briefly describe the chaotic generator that employs the NC and the mathematical model of the nonlinear converter is introduced. In Section 3 a detailed analysis of the chaotic circuit in terms of its bifurcation properties and wavelet characteristics of its time series is provided. Finally, some conclusions are presented in Section 4.

## 2.   The Chaotic Circuit

The electronic circuit of Fig. 1 (a) is known to have chaotic dynamics and has been employed to study chaos synchronization [Rulkov, 1996, Rulkov & Sushchick, 1997]. Here, we will call it as the Chaotic Generator (CG). It consists of a linear feedback and a nonlinear converter, which is the block labeled $N$, whose properties will be discussed next. The linear feedback is composed of a low-pass filter $RC'$ and a resonator circuit $rLC$.

The dynamics of the CG is very well modelled by the following set of differential equations:

$$
\begin{aligned}
\dot{x} &= y, \\
\dot{y} &= z - x - \delta y, \\
\dot{z} &= \gamma \left[ k f(x) - z \right] - \sigma y,
\end{aligned}
\tag{1}
$$

where $x(t)$ and $z(t)$ are the voltages across the capacitors, $C$ and $C'$, respectively, and $y(t) = J(t)(L/C)^{1/2}$ is the current through the inductor $L$. The unit of time is given by $\tau = 1/\sqrt{LC}$. The parameters $\gamma$, $\delta$, and $\sigma$ have the following dependence on the physical values of the circuit elements: $\gamma = \sqrt{LC}/RC'$, $\delta = r\sqrt{C/L}$ and $\sigma = C/C'$.

### 2.1.   The nonlinear converter

The main characteristic of the nonlinear converter $N$ in Fig. 1 is to transform the input voltage $x(t)$ into an output voltage with nonlinear dependence $F(x) = k f(x)$ on the input. The parameter $k$ corresponds to the gain of the converter at $x = 0$. The detailed circuit structure of $N$ is shown in Fig. 1 (b).

It is worth mentioning that depending on the component values of the linear feedback and the parameter $k$, the behavior of CG can be in regimes of either *periodic* or *chaotic* oscillations. Due to the characteristics of the inductor in the linear feedback, it turns out to be hard to scale to arbitrary frequencies and analyze it because of its frequency-dependent resistive losses. Therefore, we will focus on the parameter $k$ since as we will see it appears to be a very useful bifurcation parameter.

Figure 2 (a) shows the experimental data of $F(x)$. The nonlinear behavior of the $N$ circuit is easily obtained by turning on-off the pair of diodes.

We will briefly describe now the mathematical model for $N$ using Kirchhoff's rules. We start by employing the Shockley law for the current-voltage diagrams of the diodes

$$
i_x(V) = i_{sat} \left( e^{\eta V/T} - 1 \right) ,
\tag{2}
$$

where $i_{sat}$ is the saturation current, $T$ is the absolute thermodynamic temperature that we took as the room temperature $T = 300\,K$, $\eta = \frac{11600}{p}$ with $p$ the so-called ideality factor, which in our case is 2.

Analyzing the nonlinear module of $N$, which is enclosed in the dashed box of Fig. 1 (b), and considering standard conditions of operation, the operational amplifier $A_2$ adjusts its input voltage in order to get $V(x) := V_+ = V_-$. Using (2) one can write the current-voltage relationship as follows

$$
V(i_x) = i_x R3 + \text{sign}(i_x) \left( \frac{T}{\eta} \log \left( 1 + \frac{i_x}{i_{sat}} \right) \right) .
\tag{3}
$$

2

From Fig. 1 (b), another expression of $V(i_x)$ in terms of the input voltage $x$ can be obtained

$$V(i_x) = x - i_x R1. \tag{4}$$

Using voltage superposition, we can find the following expression of $V_-$ in terms of $F$ and $x$

$$F(x) = kf(x) = k\left(\frac{V(i_x(x)) - b_r x}{a_r}\right), \tag{5}$$

where $a_r = (R_{24})/(R5 + R_{24})$, $b_r = (R_{54})/(R2 + R_{54})$; $R_{24}$ and $R_{54}$ are the equivalent parallel resistance of $R4$ with $R2$ and $R5$, respectively. $k \in [0,1]$ corresponds to the gain in the resistor $R6$. The current $i_x(x)$ is obtained from (3) and (4). Figure 2 (b) shows the response of the mathematical model given by (5) when the values of the parameters are $k = 0.6266$, $a_r = 0.17$ and $b_r = 0.489$.

It is worth noticing that we have at our disposal a mathematical model of $F(x)$ displaying a direct relation between the parameters of equation (5) and the values of the electronic components. This is a crucial fact because it allows us to know the response of $N$ when the values of the components are changed without going to the experimental case.

## 3. Dynamical Analysis of the Chaotic Generator

In order to study the CG dynamics we consider a bifurcation analysis together with a treatment of its chaotic time series with the wavelet techniques. These methods are known to provide details about the chaotic behavior of nonlinear oscillators.

### 3.1. $k$ as a bifurcation parameter

The chaotic circuit shown in Fig. 1 was analyzed in [Campos *et al.*, 2007]. In this case, the CG was forced by an external harmonic signal $e(t) = \lambda \sin(\omega t)$, and a rich sequence of bifurcations was obtained when the bifurcation parameter $\lambda$ was increased. However, this parameter is an external parameter from the point of view of the CG.

Figure 3 (a) and (b) shows the bifurcation diagram of $x$ as a function of $k$ for the experimental and the numerical case, respectively. To get the bifurcation diagram we use a Poincaré plane $\Sigma$ defined as

$$\Sigma := \{p = (x, y, z) \in \mathbb{R}^3 : y = mx + b\}, \tag{6}$$

where $\Sigma$ is perpendicular to the $xy$ plane and intersects it at the line specified by $y = mx + b$, with $m = b = -0.1$. The value of $x$ is captured every time the flow $\varphi(x, y, z)$ of the attractor passes through the $\Sigma$ plane from the plane that does not contain the origin to the plane that contains it.

The following features are worth noticing. The oscillator dynamics may be either in a chaotic mode or in a "bistable" mode. The bistable regime is located at the values of the parameter $k$ in the range from $k_D \approx 0.19$ to $k_H \approx 0.345$. The oscillator is found in periodic orbits, for instance, a single cycle occurs for $k_D < k < 0.275$, whereas a period-doubling bifurcation develops near $k = 0.275$ and $k = 0.305$. When the interval of bistability is left, $k \geq k_H$, the attractor disappears in a saddle-node bifurcation and the oscillator turns chaotic. In fact, the CG behaves as a kind of a double-scroll oscillator. Besides, one can notice that there are several windows of periodicity between bands of chaos.

Figure 4 shows the metamorphosis of the attractors in both regimes over particular values of $k$, where the left column corresponds to experiments, whereas the right column corresponds to the numerical simulation.

Figure 5 shows the different values of $k$ as a function of $L$ at which the CG leaves the bistable region. We recall that the bistable chaos is an important active topic in the realm of the generalized synchronization of coupled chaotic systems [Guan *et al.*, 2005].

### 3.1.1. Fixed Points

We will study now the dynamics of the system (1): first, its linear part, and next, its fixed points.

*Linear part of the CG.* Any autonomous system can be written in the following form

$$x' = H(x) = Ax + G(x), \qquad H : \mathbb{R}^n \to \mathbb{R}^n \tag{7}$$

where $A$ is a linear operator ($n \times n$ real matrix) and $G(x)$ is a nonlinear function from $\mathbb{R}^n$. The linear part of the system (7) is characterized by the set of eigenvalues $\Lambda := \mathrm{spec}(A)$. The function $G$ in (7) includes all nonlinear terms of the dynamics. For the CG given by (1) the matrix $A$ and function $G$ in (7) are the following,

$$A_{CG} = \begin{pmatrix} 0 & 1 & 0 \\ -1 & -\delta & 1 \\ 0 & -\sigma & -1 \end{pmatrix}, \qquad G_{CG}(x) = \begin{pmatrix} 0 \\ 0 \\ \gamma k f(x) \end{pmatrix}, \tag{8}$$

where we will set $\sigma = 0.5007$, $\gamma = 0.3925$ and $\delta = 0.1741$. These values are given according to the components employed to realize the electronic circuit. The eigenvalues of $A$ are $\Lambda = \{-0.1515 + 1.2109i, -0.1515 - 1.2109i, -0.2636\}$. This set of eigenvalues always are the same since they do not depend on the bifurcation parameter $k$. Similarly to the Rössler system, two of the CG equations are linear and setting $z = 0$, allows examination of its dynamics on the $x - y$ plane

$$\begin{aligned} \frac{dx}{d\tau} &= y, \\ \frac{dy}{d\tau} &= -x - \delta y, \end{aligned} \tag{9}$$

The stability in the $xy$ plane can be analyzed by computing the eigenvalues of the Jacobian

$$J_{xy} = \begin{pmatrix} 0 & 1 \\ -1 & \delta \end{pmatrix}, \tag{10}$$

which are $(\delta \pm \sqrt{\delta^2 - 4})/2$. For our value of $\delta$, the eigenvalues are complex $\Lambda_{xy} := \{-0.0870 + 0.9962i, -0.0870 - 0.9962i\}$ yielding a spiral behavior on $x - y$ plane.

*The Points of Equilibrium.* From Fig. 1 one can see that when the capacitors $C$ and $C'$ have the same voltage value then the flow of the current through the inductor $L$ is zero. This implies that the current through capacitor $C$ is zero, too. Therefore, the system does not change its dynamics, as it is in a fixed point of the system. The equilibria of system (1) can be easily found by solving the system. The trivial equilibrium at $x = y = z = 0$ and the others are given symmetrically $(x, 0, x)$ such that $f(x) = (1/k)x$.

By linearizing system (1) at equilibria $S_0 = (0, 0, 0)$ and $S_{1,2} = (\pm x, 0, \pm x)$, one obtains the following characteristic polynomial

$$g(\lambda) = \lambda^3 + (\delta + \gamma)\lambda^2 + (\delta\gamma + 1)\lambda + (1 - kf')\gamma . \tag{11}$$

In order to ensure that system (1) is dissipative, just like Lorenz and Chua systems, it is required that the sum of the roots of the characteristic polynomial to be a negative quantity. For the equilibrium $S_0 = (0, 0, 0)$ to be unstable, thereby yielding a possibility for chaos, the coefficients of the characteristic polynomial (11) must satisfy the following conditions, which are obtained according to the Routh criterion:

$$\delta + \gamma > 0 \qquad \delta\gamma + 1 > 0 \qquad (1 - kf')\gamma < 0. \tag{12}$$

implying that one of the three roots of the polynomial (11) should be positive and the other two negative. It is noted that conditions (12) are necessary for system (1) to generate chaos. In table 1 the eigenvalues for different values of the bifurcation parameter $k$ are given. It is noted that condition (12) is satisfied due to $(1 - kf') < 0$. There is one positive root ($\Lambda_{S_0}$) and the system (1) is dissipative ($\sum \Lambda < 0$).

4

| $k$ | $\Lambda_{S_0} :=$ | $kf'$ | $\sum \Lambda$ |
|---|---|---|---|
| 0.3213 | $\{1.2044, -1.2805 + 2.1736i, -1.2805 - 2.1736i\}$ | 7.9040 | -1.3567 |
| 0.3223 | $\{1.2069, -1.2818 + 2.1750i, -1.2818 - 2.1750i\}$ | 7.9286 | -1.3567 |
| 0.3268 | $\{1.2180, -1.2874 + 2.1814i, -1.2874 - 2.1814i\}$ | 8.0393 | -1.3567 |
| 0.3964 | $\{1.3783, -1.3675 + 2.2758i, -1.3675 - 2.2758i\}$ | 9.7514 | -1.3567 |

Table 1: The eigenvalues of the characteristic polynomial obtained by linearizing system (1) at equilibrium $S_0$.

| $k$ | $\Lambda_{S_{1,2}} :=$ | $kf'$ | $\sum \Lambda$ |
|---|---|---|---|
| 0.3213 | $\{0.3336 + 2.1257i, 0.3336 - 2.1257i, -2.0239\}$ | $-7.4406$ | -1.3567 |
| 0.3223 | $\{0.3349 + 2.1271i, 0.3349 - 2.1271i, -2.0264\}$ | $-7.4638$ | -1.3567 |
| 0.3268 | $\{0.3406 + 2.1335i, 0.3406 - 2.1335i - 2.0378\}$ | $-7.5680$ | -1.3567 |
| 0.3964 | $\{0.4218 + 2.2267i, 0.4218 - 2.2267i, -2.2004\}$ | $-9.1798$ | -1.3567 |

Table 2: The eigenvalues of the characteristic polynomial obtained by linearizing system (1) at equilibria $S_{1,2}$.

For equilibria $S_{1,2} = (\pm x, 0, \pm x)$, the coefficients of the characteristic polynomial (11) all are positive due to $kf' < 0$. There are not any positive real values. Now, one of the three eigenvalues of equation (11) is a negative real value, and the other two are complex with a positive real part. In table 2 the eigenvalues for different values of the bifurcation parameter $k$ are given.

These eigenvalues have the following implications: first, the two eigenvalues $\Lambda_{S_{1,2}}$ are responsible for the steady outward slide, and the last eigenvalue is attracting; second, the system (1) is dissipative ($\sum \Lambda < 0$).

Figure 6 shows the nonlinear function and the line $(1/k)x$ for several values of the bifurcation parameter $k$. The equilibria $(\pm x, 0, \pm x)$ are defined as the intersections of $f(x)$ and $(1/k)x$. The bifurcation parameter $k$ belongs to the closed interval $[0, 1]$, due to it is related to a potentiometer. For values of the bifurcation parameter $k = 1$ (dashed line), $k = 0.3218$ (solid line) and $k = 0.045$ (dotted line), the intersections are approximately $x_M = 1.04$, $x_B = 0.94$ and $x_F = 0.04$, respectively. Then, the equilibrium points are given for values of $x$ in the interval $(0.04, 1.04)$. These equilibrium points define the dynamics of the system 1 in two intervals: $(0.4, 0.94)$ in which there are two attractors and $(0.94, 1.04)$ with one attractor.

## 3.2.  The CG as an equivalent Chua's oscillator

The nonlinear converter exhibits a rich dynamics with many different attractors. In this subsection, by means of the algorithm provided in [Chua, 1993, Chua *et al.*, 1993], we give a set of parameter values for which the dynamics of the CG system can be mapped into that of a Chua's oscillator, in other words, our oscillator is topologically conjugate to a particular unfolded Chua's circuit. In [Chua, 1993, Chua *et al.*, 1993], it is shown and described how Chua's circuit is topologically conjugate to a large class of 3rd-order chaotic systems whose dynamical behavior is determined by two sets of eigenvalues, $\mu_i$ and $\nu_i$, $i = 1, 2, 3$, corresponding to the characteristic polynomials associated to the inner and outer regions, respectively, of the vector field for a three-segment piecewise linear function by which we can approximate $F(x)$.

First of all, we look for a good approximation of our $F(x)$ to one of the three-segment piecewise-linear functions characterizing the nonlinear Chua resistor in the unfolded Chua's circuit, i.e., that in Fig. 2 (e) of [Chua, 1993]. To achieve this, we use the eigenvalues given in the last row of the Tables I and II corresponding to the inner and outer regions of the three-segment piecewise-linear function generating the attractors displayed in Fig. 4 (g) and (h).

Following the algorithm presented in [Chua, 1993, Chua *et al.*, 1993], the equivalent Chua's eigenvalue parameters are

$$\begin{cases} p_1 & = -1.3567, \quad p_2 \quad = 3.2797, \quad p_3 \quad = 9.7157 \; , \\ q_1 & = -1.3567, \quad q_2 \quad = 3.2797, \quad q_3 \quad = -11.3013 \; . \end{cases} \tag{13}$$

Since $p_1 = q_1$, we add a small perturbation $\delta p_1 = 0.1018$ and $\delta q_1 = -0.1018$ obtaining

$$\begin{cases} p_1 & = -1.2550, \quad p_2 \quad = 3.2797, \quad p_3 \quad = 9.7157 \; , \\ q_1 & = -1.4585, \quad q_2 \quad = 3.2797, \quad q_3 \quad = -11.3013 \; . \end{cases} \tag{14}$$

We are thus able to show that the CG circuit is topologically conjugate to Chua's unfolded circuit for the following set of parameter values

$$\begin{cases} C_1 & = 1.0000, \\ C_2 & = 51.5099, \\ L & = 1.8452 \times 10^{-4}, \\ R & = -0.0139, \\ R_0 & = 2.5708 \times 10^{-4}, \\ G_a & = 73.0231, \\ G_b & = 73.2267. \end{cases} \tag{15}$$

Notice from Fig. 7 (a) that while doing the approximation, the two horizontal segments of $F(x)$ have been deleted because they correspond to the saturation regime which is not of interest in this mapping.

Using now the parameters in (15), we obtain the attractor of Fig. 7 (b) which is of similar shape to the attractor 11 of [Chua *et al.*, 1993]. This proves Chua's topologically conjugated property for our CG model.

## 3.3. Time series

In order to analyze the numerical time series of the CG, we consider the log variance of the wavelet coefficients as a function of level $m$ following our previous work [Murguía & Campos–Cantón, 2006]. It is known that the wavelet variance provides a very efficient measure of the structure contained within a time series because of the ability of wavelet transforms to allot small wavelet coefficients to the smoother parts of a signal in contrast with the sharp, non-stationary behavior which gives rise to local maxima (see, for example, Chapter 8 in the book of Percival and Walden [Percival & Walden, 2000]).

### 3.3.1. Wavelet approach: a short introduction

There are numerous integral transforms for signal processing, but there is more and more consensus that the *wavelet transforms* allow to obtain more detailed pieces of information about signals. These transforms using integration kernels called wavelets are known to be useful in handling non stationary and transient signals, as well as fractal-type structures [Murguía & Campos–Cantón, 2006].

Due to the fact that some data are represented by a finite number of values, we consider the orthogonal (discrete) wavelet case in which the wavelets are associated to orthonormal bases of $L^2(\mathbb{R})$. First, a discrete grid is established for the dilation and translation parameters such that the orthonormal wavelet basis functions can be expressed in the form

$$\psi_{m,n}(t) = 2^{m/2}\psi(2^m t - n), \tag{16}$$

with $m$ and $n$ denoting the dilation and translation indices, respectively. Within this framework, one can write the expansion of an arbitrary signal $x(t)$ in an orthonormal wavelet basis as follows

$$x(t) = \sum_m \sum_n x_n^m \psi_{m,n}(t), \tag{17}$$

where the coefficients of the expansion are given by

$$x_n^m = \int_{-\infty}^{\infty} x(t)\psi_{m,n}(t)dt \; . \tag{18}$$

The contribution of the signal at a particular wavelet level $m$ is given by

$$x_m(t) = \sum_n x_n^m \psi_{m,n}(t). \tag{19}$$

Equation (19) gives us information of the time behavior of the signal within different scale bands, and in addition provides us with their contribution to the total signal energy. We associate higher levels with higher scales, as discussed in Refs. [Murguía & Campos–Cantón, 2006, Staszewski & Worden, 1992].

As discussed in Ref. [Wornell & Oppenheim, 1992], some degree of regularity is useful on the wavelet basis to have a well-behaved representation. To achieve this, a wavelet function should have $p$ vanishing moments. A wavelet is said to have $p$ vanishing moments, and denoted as $\psi_p(t)$, if and only if it satisfies

$$\int_{-\infty}^{\infty} t^k \psi_p(t) dt = 0, \tag{20}$$

for $\quad k = 0, 1, \ldots, p - 1$, and

$$\int_{-\infty}^{\infty} t^k \psi_p(t) dt \neq 0, \quad \text{for} \quad k = p.$$

This means that a wavelet with $p$ vanishing moments is orthogonal to polynomials up to order $p - 1$. Thus the wavelet transform of $x(t)$ with a wavelet $\psi_p(t)$ is nothing but a "smoothed version" of the $p$–th derivative of $x(t)$ on various scales. In fact, when someone is interested to measure the local regularity of a signal this concept is of fundamental importance [Daubechies, 1992, Mallat, 1999].

The Daubechies wavelets are the analyzing wavelet functions that we use in this paper. These wavelets are determined recursively from their scaling function and are compactly supported. They are termed as DaubN and written as $dbN$, where $N$ corresponds to the order of the function. Some authors use $2N$ instead of $N$. More details about this important class of wavelets can be found in [Daubechies, 1992, Mallat, 1999].

In the wavelet approach the fractal character of a certain signal can be inferred from the behavior of its power spectrum $P(\omega)$, which is the Fourier transform of the autocorrelation function and in differential form $P(\omega)d\omega$ represents the contribution to the variance of a signal from frequencies between $\omega$ and $\omega + d\omega$. Indeed, it is known that for self-similar random processes the spectral behavior of the power spectrum is given by

$$P(\omega) \sim \mid \omega \mid^{-\gamma}, \tag{21}$$

where $\gamma$ is the spectral parameter of the wave signal. In addition, the variance of the wavelet coefficients Var $\{x_n^m\}$ is related to the level $m$ through a power law of the type [Wornell & Oppenheim, 1992]

$$\text{Var} \ \{x_n^m\} \approx (2^m)^{-\gamma}. \tag{22}$$

This wavelet variance is used to find dominant levels associated with the signal, for example, in the study of chaotic time series [Murguía & Campos–Cantón, 2006, Staszewski & Worden, 1992].

### 3.3.2. Maxima in the variance plots

Equation (22) is certainly suitable for studying discrete chaotic time series because their variance plot has a well defined form as pointed out in Refs. [Murguía & Campos–Cantón, 2006, Staszewski & Worden, 1992]. If the variance plot shows a maximum in a particular scale, which means an energy concentration, it will often corresponds to a coherent structure. In general, the gradient of a noise time series turns out to be zero in the variance plot, therefore it does not show any energy concentration at specific wavelet level. In certain cases the gradient of some chaotic time series has a similar appearance with Gaussian noise at lower scales, which implies that these chaotic time series do not present a fundamental "carrier" frequency at any scale.

For our illustrative analysis and comparison with the experiments, we start with the time series of the attractors displayed in Fig. 8 as well as the attractor in Fig. 4 (h, g) because they are of very different type and we want to emphasize the versatility of the wavelet approach. Fig. 8 (a,b) corresponds to $k = 0.3045$ when the experimental and numerical CGs generate thin, periodic attractors. On the other hand, at $k = 0.4010$, Fig. 8 (c,d) shows an attractor (again, experimental and numerical, respectively) that takes a similar shape to a Rössler attractor. Moreover, for $k = 0.3964$ (see Fig. 4 (g,h)), the CG generates an attractor with a shape similar to a double scroll oscillator. For the acquisition of the experimental data we used a DAQ with a sampling frequency of 180 kHz, i.e., we collected the experimental data for a total time of 182 ms in all cases. The numerical data have been simulated using a fourth-order Runge-Kutta scheme with a step size equal to $h = 0.005$ and 32768 points, or 65536 points, after transients, were obtained. In the analysis of all time series we employed $db8$ wavelets. The number of samples used in the numerical approximation has been estimated from the relationship $n = \tau(hT_s)^{-1}$, where $\tau$ is the time constant of the circuit, $h$ is the numerical step size, and $T_s = 1.8 \times 10^{-5}$ is the experimental sampling period.

- Case $k = 0.3045$.

  The first time series to consider corresponds to the $x$ state of the experimental attractor of Fig. 8 (a). This time series is shown in Fig. 9 (a), where we can notice a kind of "periodic" orbit, whereas Fig. 9 (b) shows a semi-logarithmic plot of the wavelet coefficient variance as a function of level $m$.

  At level $m = 11$ a pronounced peak occurs indicating a concentration of energy at this wavelet level with a downward shift because of the DC component of this time series. The energy in this level is approximately equal to 93% and in fact almost all the rest of the energy is concentrated in the two adjacent levels to $m = 11$, i.e., $m = 10$ and $m = 12$. The reconstruction of the signal at level 11 is shown in Fig. (9) (c) and for the sum of three levels 10-12 in Fig. (9) (d). The corresponding errors for these reconstructions are displayed in Fig. (9) (e,f), respectively. The same analysis is accomplished in the corresponding numerical case. The results are shown in Fig. (10) (a-f) and are in very good agreement with the experiment.

- Case $k = 0.4010$.

  The time series shown in Figs. 11 (a) and 12 (a) correspond respectively to the experimental and numerical $x$ state of the attractors shown in Fig. 8 (c,d). Starting with the experimental case, the variance plot of the wavelet coefficients is shown in Fig. 11 (b), and one can notice that the whole series is dominated by the 12th level with a slight downward shift due to the DC component. The energy in this wavelet level is close to 96% of the total one in this case. If the three maxima wavelet levels $m = 11 - 13$ are added together, their energy concentration reaches already 99% of the total. The reconstruction of the signal at level 12 is shown in Fig. (11) (c) and for the sum of the three levels 11-13 in Fig. (11) (d). The corresponding errors for these reconstructions are displayed in Fig. (11) (e,f), respectively.

  The same analysis is accomplished in the corresponding numerical case with the results displayed in Fig. (12) (a-f). One can notice a very good agreement with the experiment.

  On the other hand, we also analyzed the experimental and numerical time series of the $z$ state of the same attractor in Figs 13 and 14, respectively. In the experimental case, Fig. 13 (a) shows the time series, (b) the variance plot, (c) the 12th wavelet level, and (d) the sum of levels $m = 11 - 13$. A well-developed maximum occurs at level $m = 12$, with an energy contribution near 92%, and again more than 99 % of the energy concentration is reached for the same three levels as before. All these experimental facts are obtained very similarly in the numerical case as seen in Fig. 14.

  It is worth noting that in both states $x$ and $z$, the energy concentration has a similar distribution indicating that the chaotic behavior is independent of state for this attractor.

- Case $k = 0.3964$.

  At this value of $k$, the CG behaves as a double scroll oscillator with the shape of the attractor displayed in Fig. 4 (g,h). The experimental time series corresponding to the $x$ state of this attractor

is shown in Fig. 15 (a), while the variance plot is given in Fig. 15 (b) where no representative energy concentration can be seen. To get a substantial component of this time series, we have to sum over seven wavelet levels, $m = 6 - 12$, for which the energy contribution is close to 99% of the total but without any pronounced peak. According to our previous remarks, this case does not present a fundamental "carrier" frequency and therefore this attractor has a Gaussian noisy behavior. As in the previous cases, we performed the numerical analysis displayed in Fig. 16 finding a very good agreement with the experimental case for this attractor as well.

We thus have shown here that despite the presence of different kinds of attractors in the CG, the wavelet analysis of their time series is very informative for all of them proving the flexibility of this tool.

## 4. Conclusions

We have introduced a mathematical model for the nonlinear converter of Rulkov *et al* [Rulkov, 1996] which is better adapted to a direct relationship with the components employed to build experimentally the nonlinear converter. This model allows us to analyze in detail the CG chaotic behavior. We present quantitative accurate measurements of the system by comparing the bifurcation diagrams obtained from the different attractors that occur while varying the parameter $k$ with their computer simulation counterparts. Depending on the value of $k$, the behavior of CG can set in regimes of either periodic or chaotic oscillations thus establishing $k$ as a good bifurcation parameter. In a general way, the bifurcation diagram reveals that at low values of $k$ the attractors are periodic, but quickly they become chaotic as $k$ increases. Besides, a bistable regime sets up at a certain range of values of the parameters $k$ and $L$ that can be useful in generalized synchronization research [Guan *et al.*, 2005]. In addition, we show that the dynamics of the CG circuit can be mapped to that of the unfolded Chua circuit and therefore the modeled CG belongs to the large class of Chua's topologically conjugated three-dimensional systems.

Moreover, an important contribution in this paper is that a standard wavelet transform is used to analyze the experimental and numerical CG chaotic time series. It appears that the wavelet procedure is a very illustrative means of revealing characteristic variations at different scales and for separating structured variations from the stochastic ones. For example, for periodic and Rössler type attractors, we report a strong energy concentration in a few wavelet levels, which we interpret as the carrier frequencies of the chaotic time series. On the other hand, for the chaotic time series of a double-scroll type attractor we have found a noisy behavior and a nearly zero gradient of the log variance of the wavelet coefficients at lower scales.

# References

Abarbanel, H. D. I., Frison, T. W., & Tsimring, L. S. [1993] "Obtaining order in a world of chaos: time-domain analysis of nonlinear and chaotic signals," *IEEE Signal Processing Magazine*, **15**(3), 49–65.

Carroll, T.L. & Pecora, L. M. [1992] "A circuit for studying the synchronization of chaotic systems," *Int. J. Bifurcation and Chaos* **2**(3), 659–667.

Carroll, T. L. [1995] "A simple circuit for demonstrating regular and synchronized chaos," *Am. J. Phys.* **63**(4), 377–379.

Campos-Cantón, E., González, J. S. & Urías, J. [2007] "Poincaré planes in nonlinear electronics," *Int. J. Bifurcation and Chaos* **17**(1), 199-208.

Chua, L. O., Kocarev, L., Eckert, K. & Itoh, M. [1992] "Experimental chaos synchronization in Chua's circuit," *Int. J. Bifurcation and Chaos* **2**(3), 705-708.

Chua, L. O. [1993] "Global unfolding of Chua's circuit," *IEICE Trans. Fundamentals* **E76-A**(5), 704-734.

Chua, L. O., Wu, C. W., Huang, A., & Zhang, G.-Q. [1993] "A universal circuit for studying and generating chaos- part II: Strange attractors," *IEEE Trans. on Circuits and Systems*, **40**(10), 745–761.

Daubechies, I. [1992] *Ten Lectures on Wavelets* (SIAM, Philadelphia).

Guan, S., Lai, C.-H. & Wei, G. W. [2005] "Bistable chaos without symmetry in generalized synchronization" *Phys. Rev. E* **71**, 036209.

Kiers, K., Schmidt, D. & Sprott, J. C. [2004] "Precision measurements of a single chaotic circuit," *Am. J. Phys.* **72**(4), 503-509.

Mallat, S. [1999] *A Wavelet Tour of Signal Processing* (2nd Edition, Academic Press).

Murguía, J. S. & E. Campos-Cantón, E. [2006] "Wavelet analysis of chaotic time series," *Rev. Mex. Fís.* **52**(2), 155-162.

Percival, D. B. & Walden, A. T. [2000] *Wavelet Methods for Time Series* (Cambridge University Press, Cambridge).

Rulkov, N. F. [1996] "Images of synchronized chaos: Experiments with circuits," *Chaos* **6**(3), 262-279.

Rulkov, N. F. & Sushchik, M. M. [1997] "Robustness of Synchronized Chaotic Oscillations," *Int. J. Bifurcation and Chaos* **7**(3), 625-643.

Rulkov, N. F., Afraimovich, V. S., Lewis, C. T., Chazottes, J. R. & Cordonet, A. [2001] "Multivalued mappings in generalized chaos synchronization," *Phys. Rev. E* **64**, 016217.

Staszewski, W. J. & Worden, K. [1999] "Wavelet analysis of time series: Coherent structures, chaos and noise," *Int. J. of Bifurcation and Chaos*, **9**(3), 455-471.

Sprott, J. C. & Linz, S. J. [2000] "Algebraically simple chaotic flows," *Int. J. of Chaos Theory and Applications* **5**, 3-22.

Sprott, J. C. [2000] "A new class of chaotic circuit," *Phys. Lett. A* **266**, 19-23.

Wornell, G. W. & Oppenheim, A. V. [1992] "Wavelet-based representations for a class of self-similar signals with application to fractal modulation," *IEEE Trans. Inform. Theory* **38**(2), 785–800.
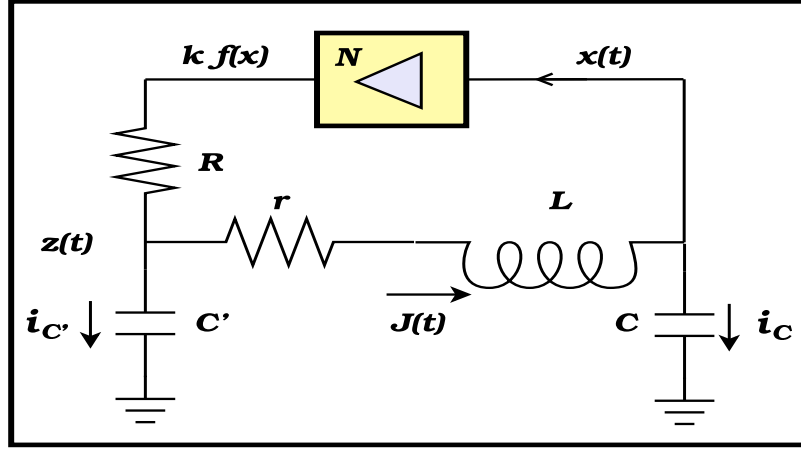
**(a)**
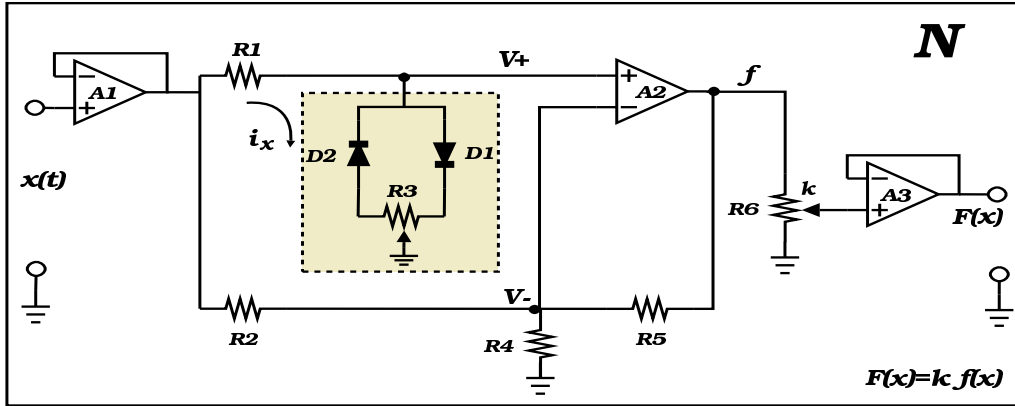


**(b)**

Figure 1: (Color online) (a) The circuit diagram of the chaotic oscillator. The component values employed are $C' = 100.2$ nF, $C = 200.1$ nF, $L = 63.8$ mH, $r = 138.9$ $\Omega$, and $R = 1018$ $\Omega$. (b) Schematic diagram of the nonlinear converter N. The electronic component values are $R1 = 2.7$ k$\Omega$, $R2 = R4 = 7.5$ k$\Omega$, $R3 = 50$ $\Omega$, $R5 = 177$ k$\Omega$, $R6 = 20$ k$\Omega$. The diodes D1 and D2 are 1N4148, the operational amplifiers A1 and A2 are both TL082, and the operational amplifier A3 is LF356N.
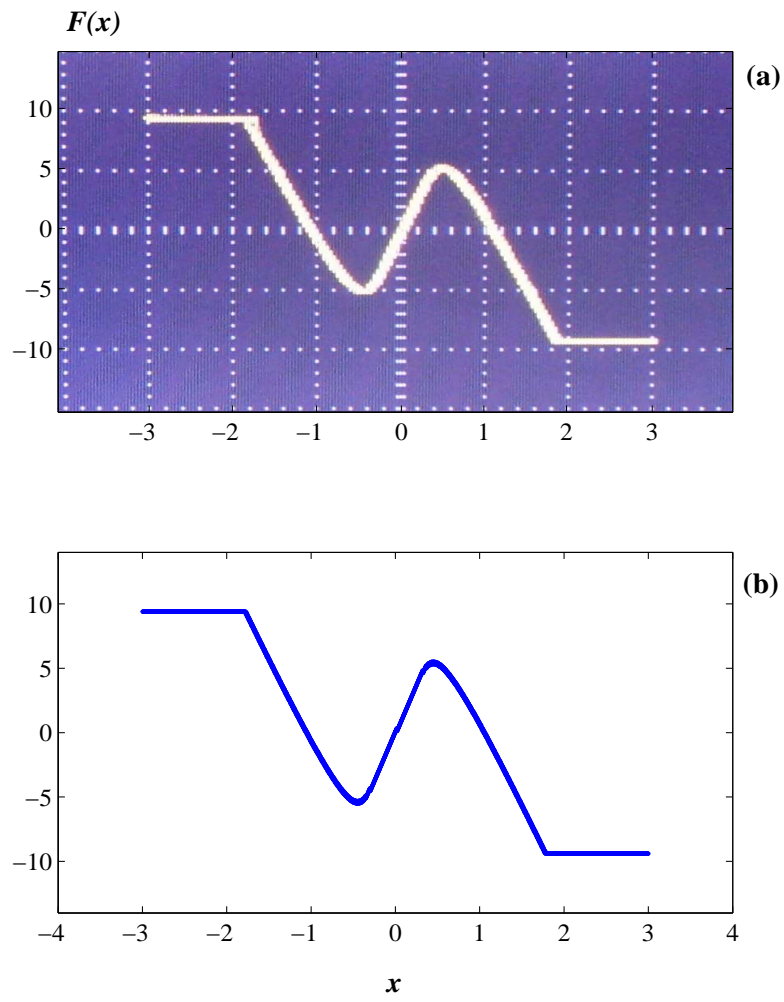
Figure 2: (Color online) The characteristic response curves of the nonlinear converter $N$, (a) from the experimental circuit, and (b) from Eq. (5) for $k = 0.6266$, $a_r = 0.17$ and $b_r = 0.489$.
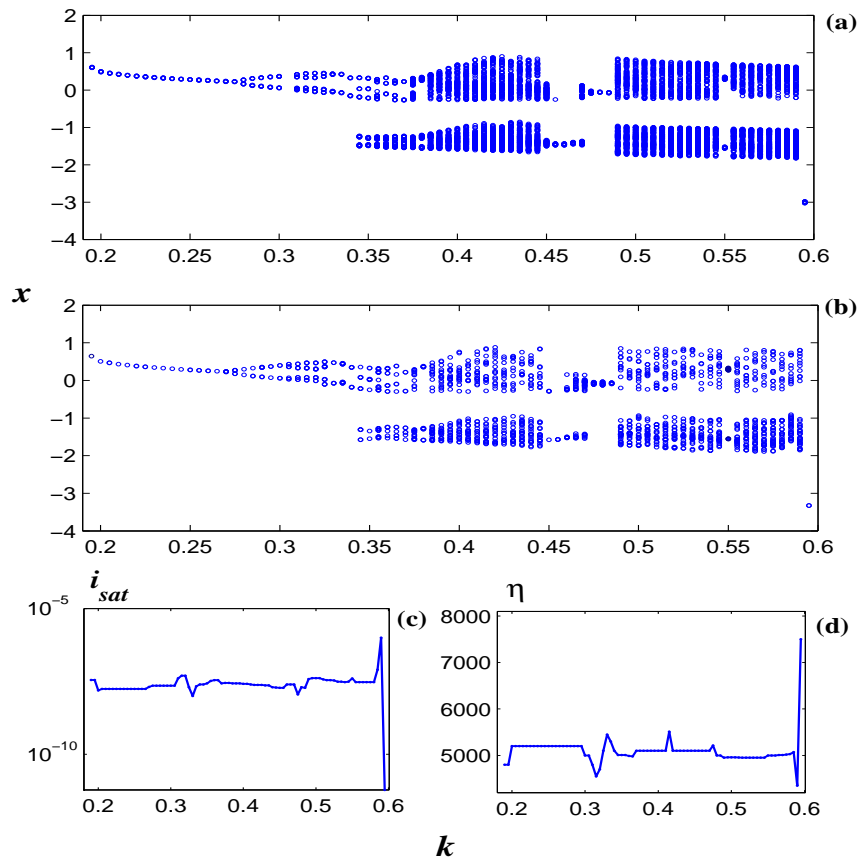
Figure 3: (Color online) State $x$ against parameter $k$ for the bifurcation diagram of the CG with $L = 63.8$ mH: (a) the experimental data, (b) the numerical approximation, (c) and (d) refer to the parameters in Shockley's law used in the numerical approximation.
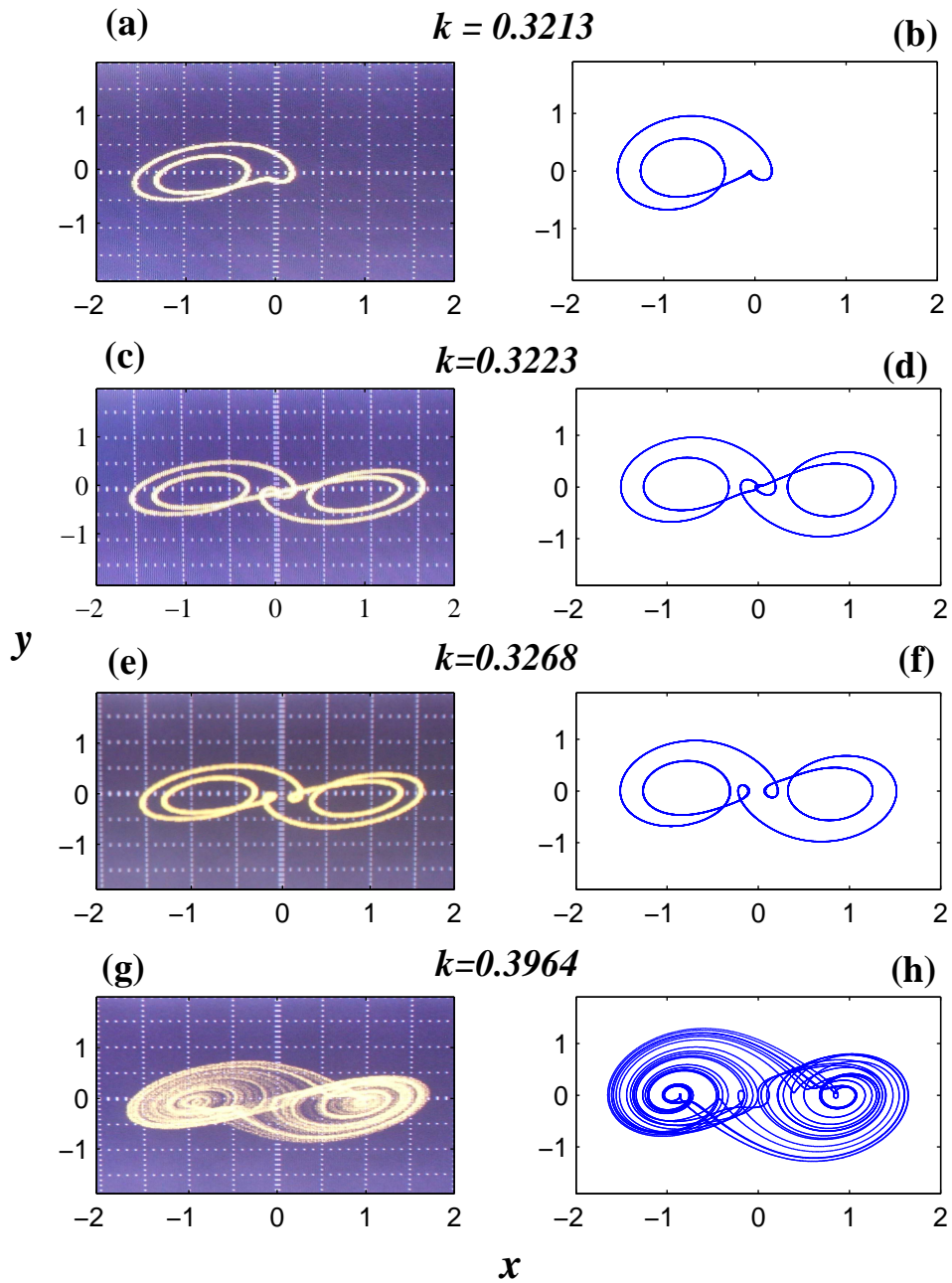
Figure 4: (Color online) Different attractors obtained varying the parameter $k$. The left column shows experimental attractors, whereas the right one displays their numerical counterparts for the same value of the parameter $k$.
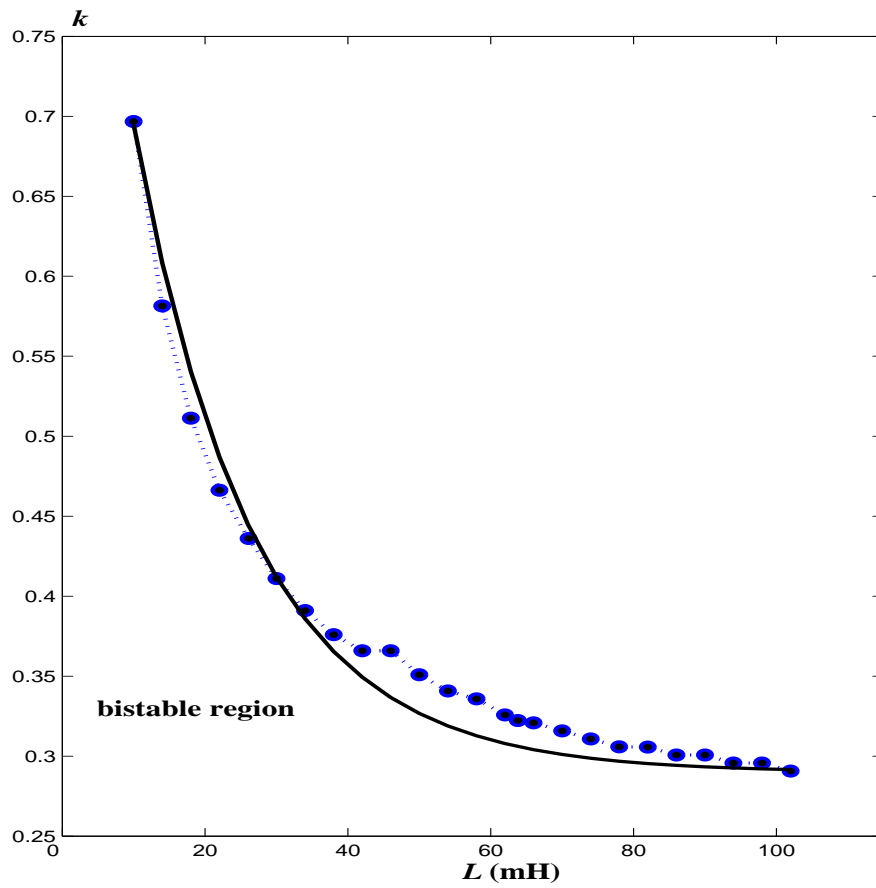
Figure 5: (Color online) Values of $k$ as a function of $L$. The dashed line with points displays the numerical values for which the CG left the bistable region. The solid curve is an approximation given by a decreasing exponential function.
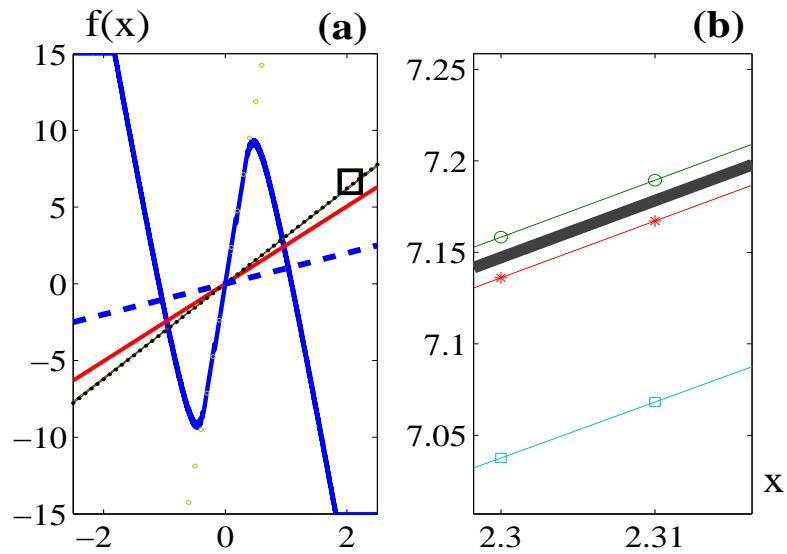
Figure 6: (Color online) (a) The nonlinear function $f(x)$ and the line $(1/k)x$ for different values of bifurcation parameter $k$: 0.0421 (circle line), 0.3218 (dotted line), 0.3965 (solid line) and 1 (dashed line); (b) a zoom on the rectangle shown in (a) for $k$: 0.3213 (line with circles), 0.3218 (solid line), 0.3223 (line with asterisks), and 0.3268 (line with squares).
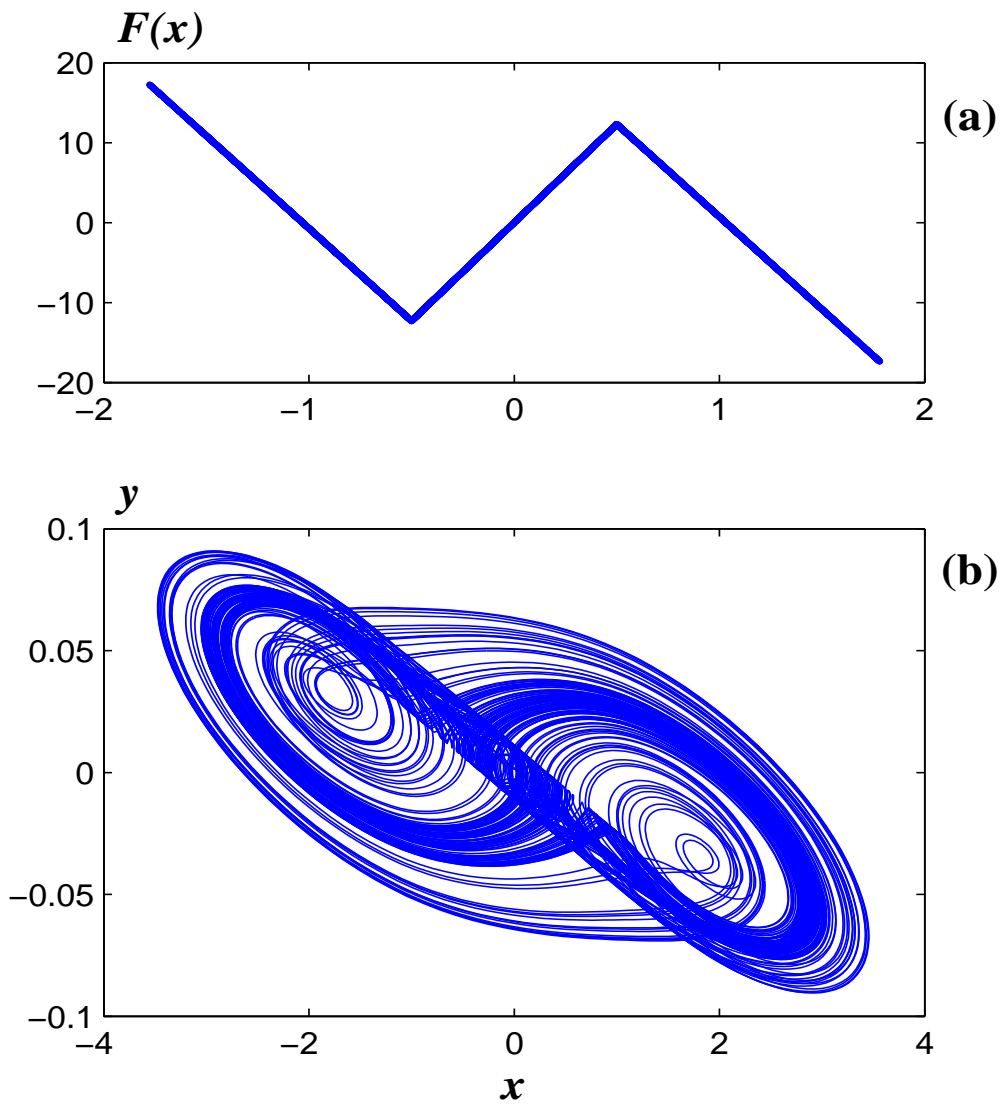
Figure 7: (Color online) The characteristic response curve of the nonlinear converter $N$ for the bifurcation parameter $k = 0.3964$ (a) and (b) the corresponding equivalent strange attractor generated by the unfolded Chua's circuit.
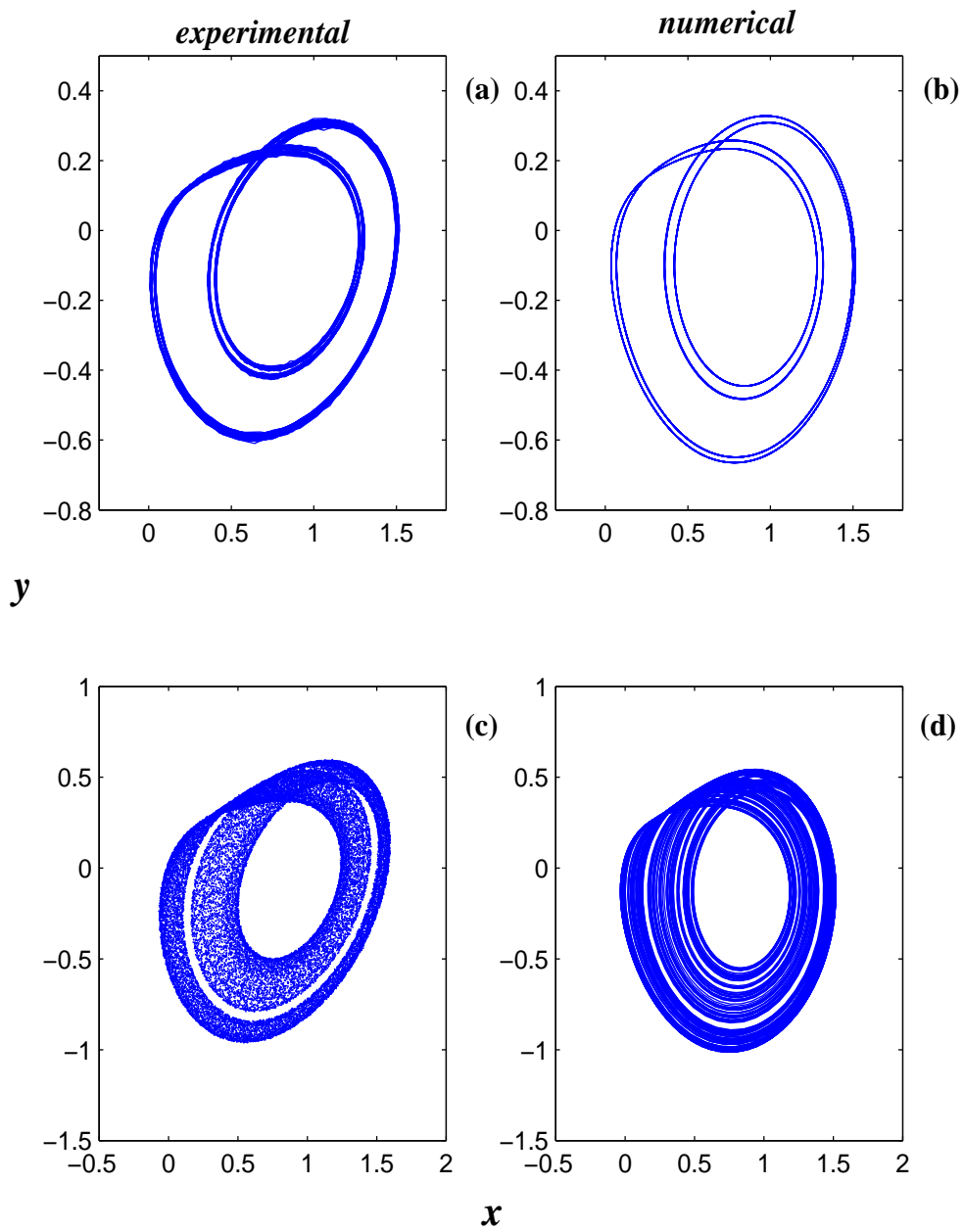
Figure 8: (Color online) Attractors of the CG projected on the plane $x - y$ obtained experimentally and numerically for different values of the bifurcation parameter $k$: (a) and (b) 0.3045, and (c) and (d) 0.4010 (with $L = 26.1$ mH).
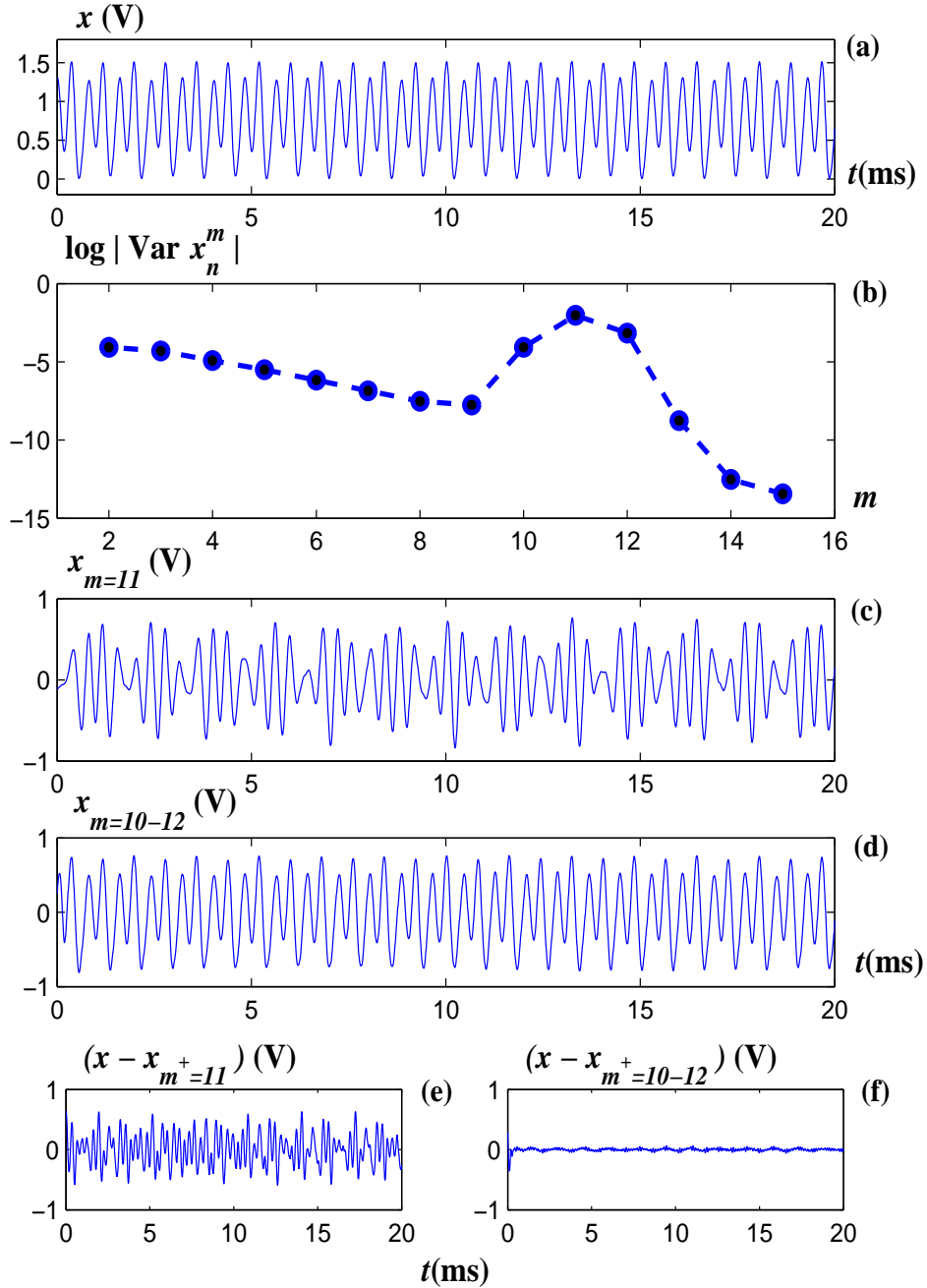
Figure 9: (Color online) For $k = 0.3045$: (a) experimental time series of the $x$ state, (b) wavelet coefficient variance, (c) the time series of the 11th wavelet level, (d) the time series of the sum from 10th to the 12 wavelet levels, (e) and (f) the corresponding experimental errors between (a) and (c) and (a) and (d), respectively.
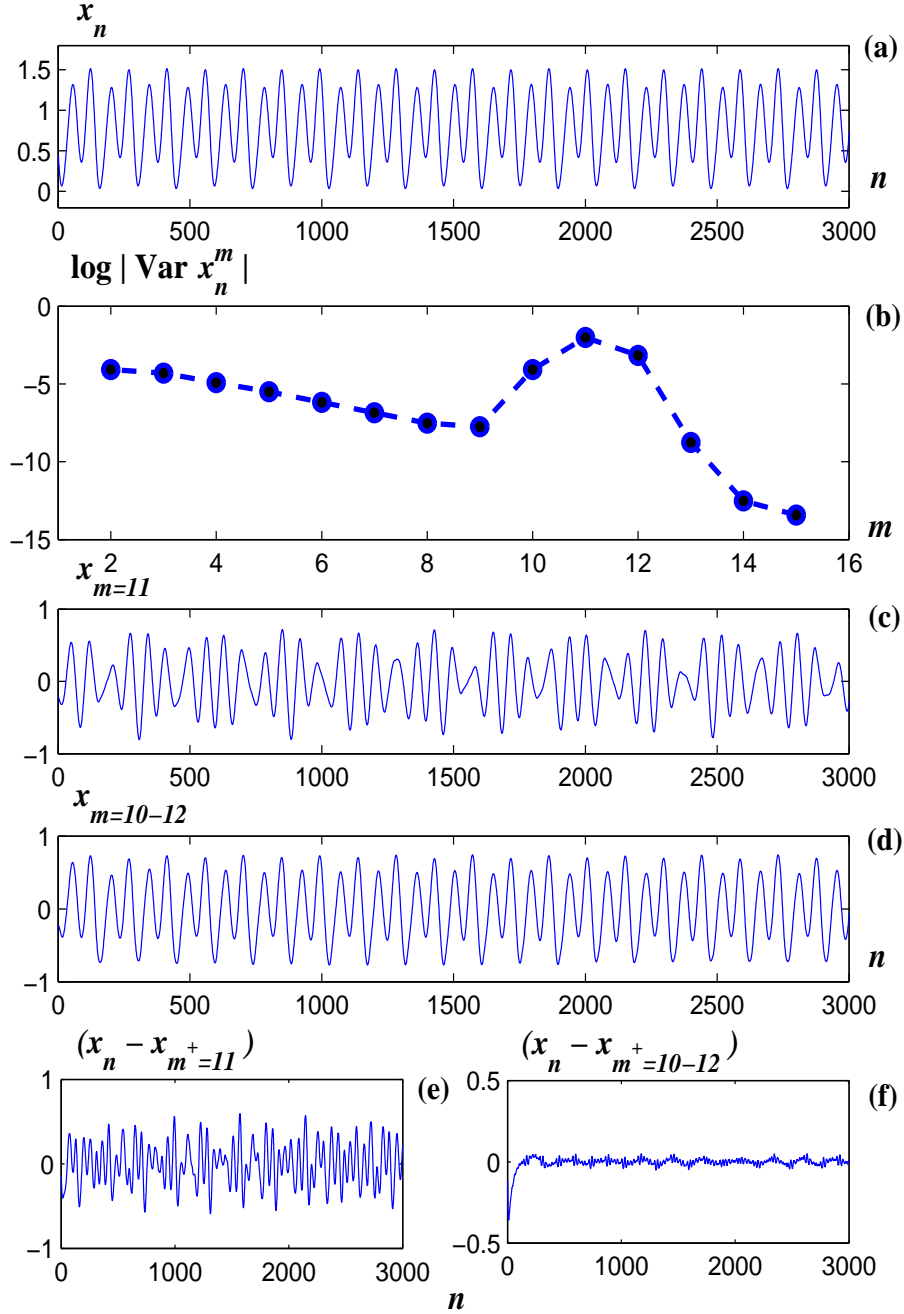
Figure 10: (Color online) For $k = 0.3045$: (a) numerical time series of the $x$ state, (b) wavelet coefficient variance, (c) the time series of the 11th wavelet level, (d) the time series of the sum from 10th to the 12 wavelet levels, (e) and (f) the corresponding numerical errors between (a) and (c) and (a) and (d), respectively.

20
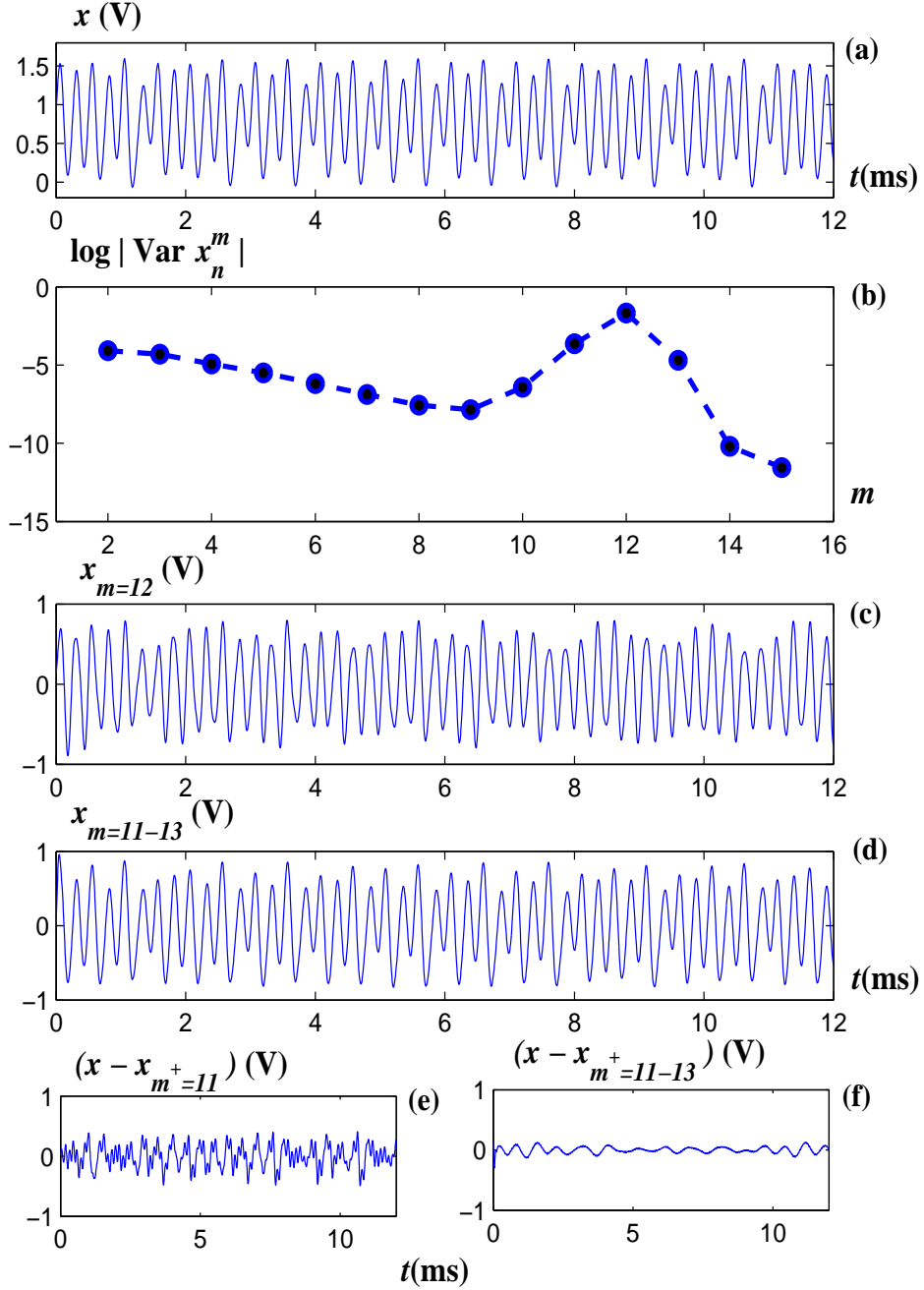
Figure 11: (Color online) The case $k = 0.4010$: (a) experimental time series of the $x$ state, (b) wavelet coefficient variance, (c) the time series of the 12th wavelet level, (d) the time series of the sum from 11th to the 13 wavelet levels, (e) and (f) the corresponding experimental errors between (a) and (c) and (a) and (d), respectively.

21
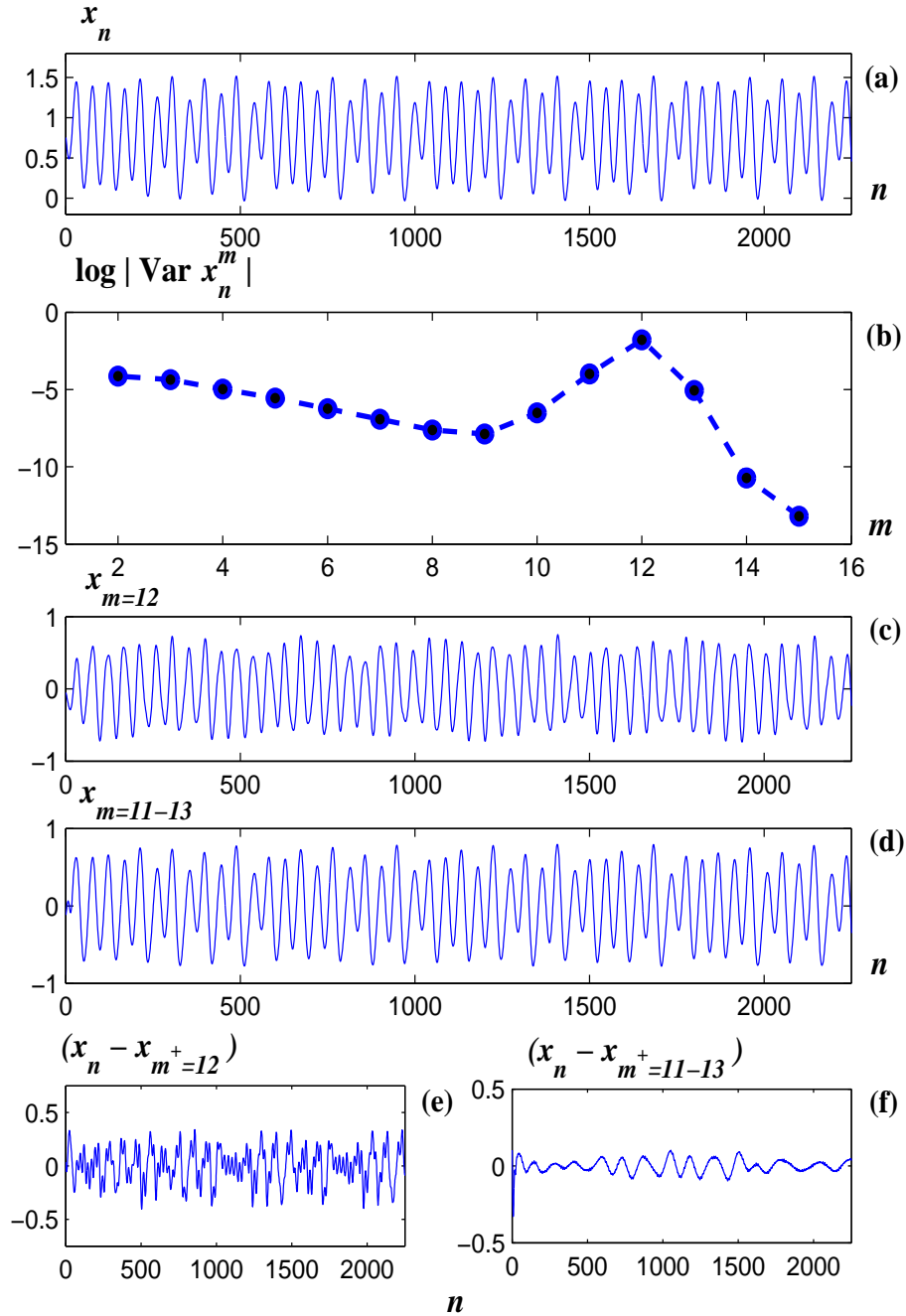
Figure 12: (Color online) The case $k = 0.4010$: (a) numerical time series of the $x$ state, (b) wavelet coefficient variance, (c) the time series of the 12th wavelet level, (d) the time series of the sum from 11th to the 13 wavelet levels, (e) and (f) the corresponding numerical errors between (a) and (c) and (a) and (d), respectively.

22
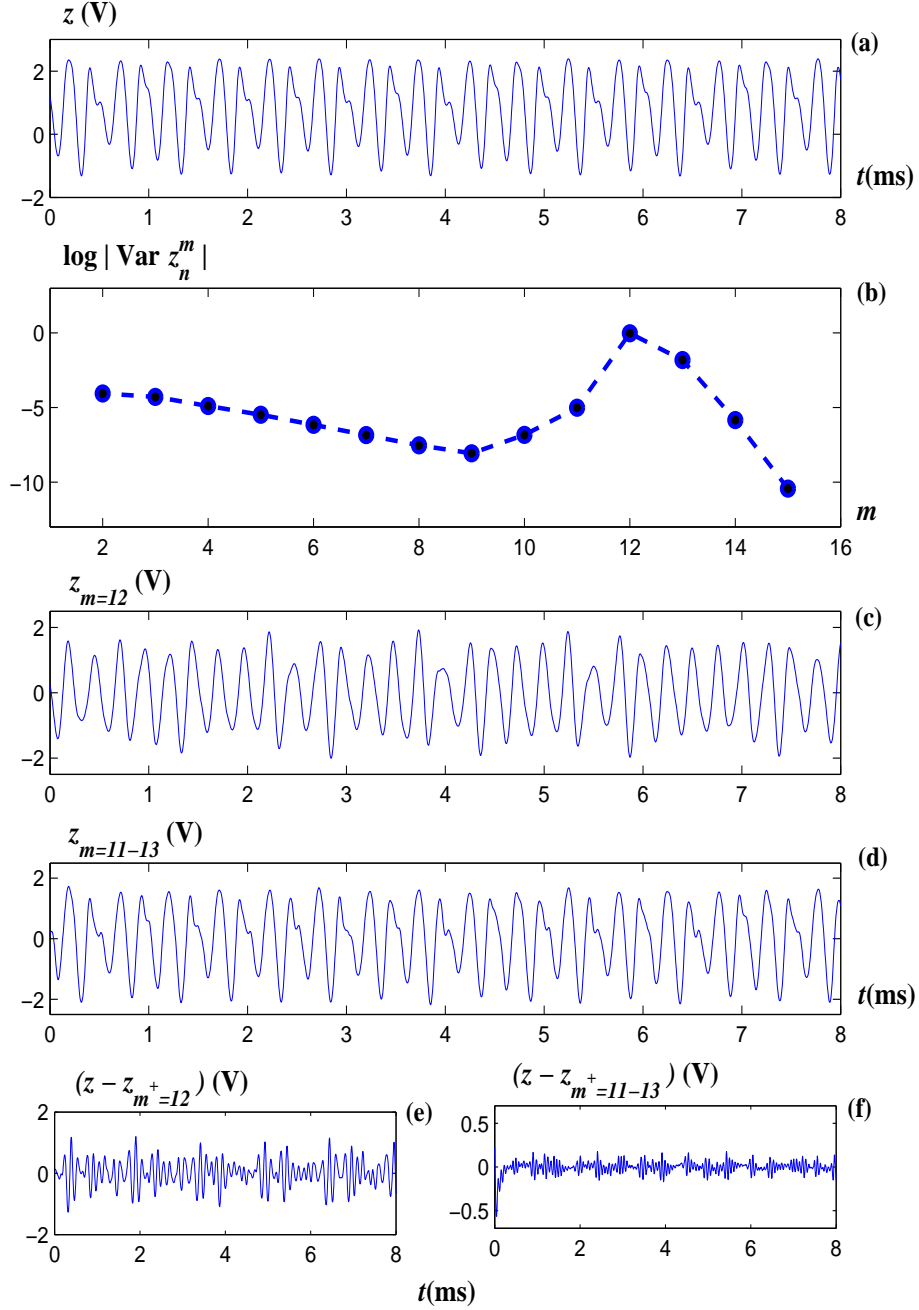
Figure 13: (Color online) The case $k = 0.4010$: (a) experimental time series of the $z$ state, (b) wavelet coefficient variance, (c) time series of the 12th wavelet level, (d) the time series of the sum from 11th to the 13 wavelet levels, (e) and (f) the corresponding experimental errors between (a) and (c) and (a) and (d), respectively.
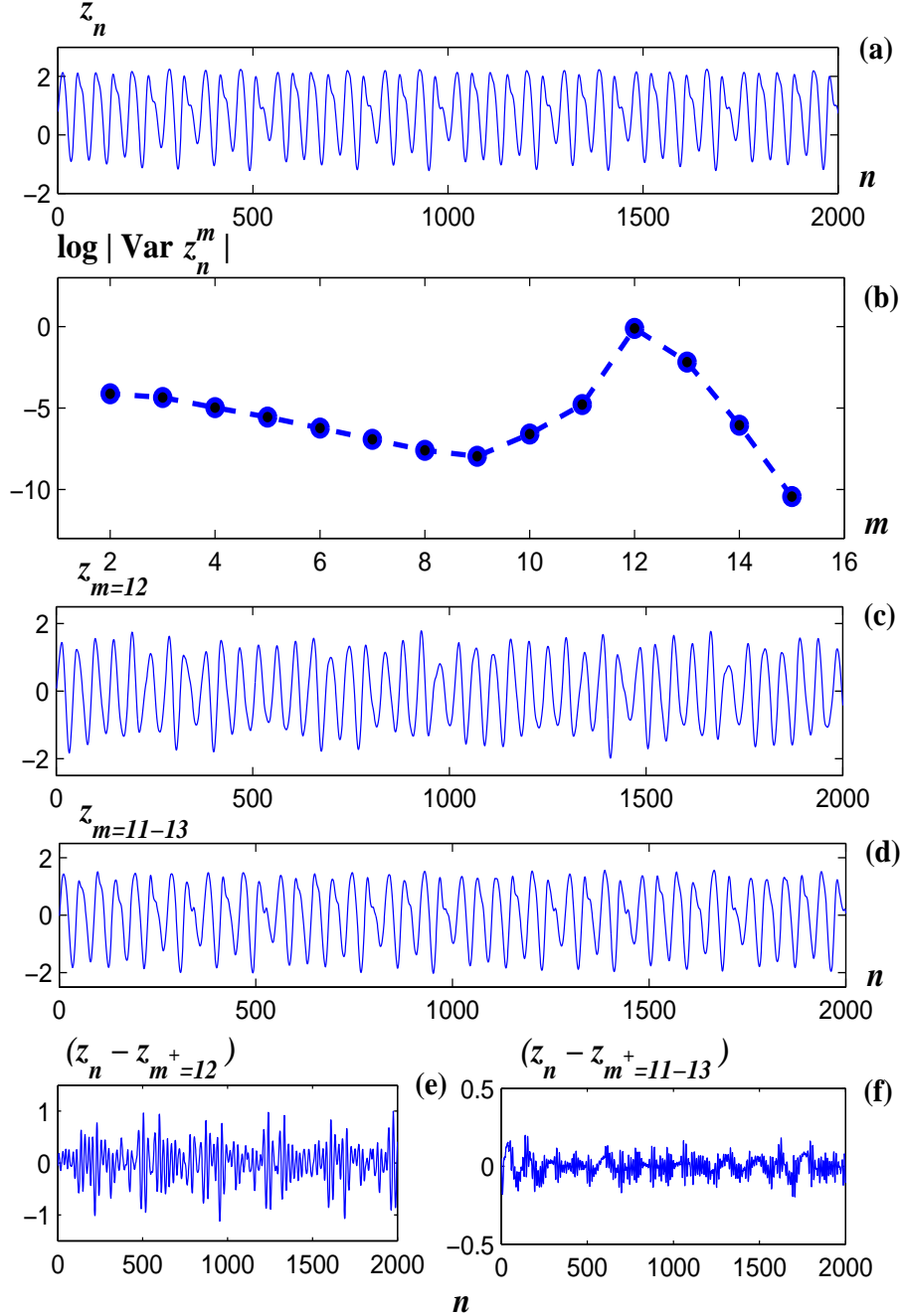
Figure 14: (Color online) The case $k = 0.4010$: (a) numerical time series of the $z$ state, (b) wavelet coefficient variance, (c) time series of the 12th wavelet level, (d) the time series of the sum from 11th to the 13 wavelet levels, (e) and (f) the corresponding numerical errors between (a) and (c) and (a) and (d), respectively.
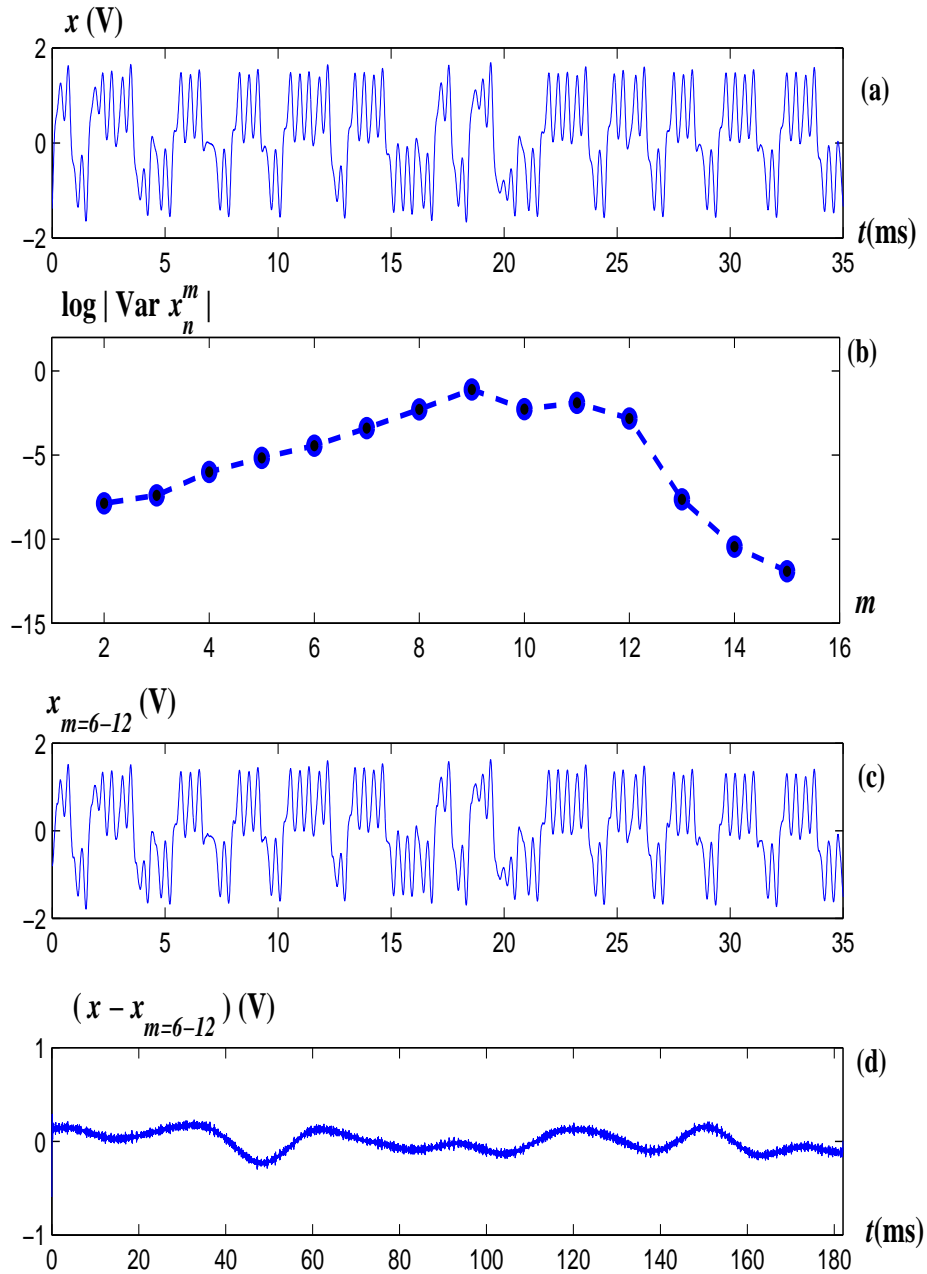
Figure 15: (Color online) The case $k = 0.3964$: (a) experimental time series of the $x$ state, (b) wavelet coefficient variance, (c) time series for the sum of the 6th to the 12th wavelet levels of the $x$ series, and (d) experimental errors between (a) and (c).
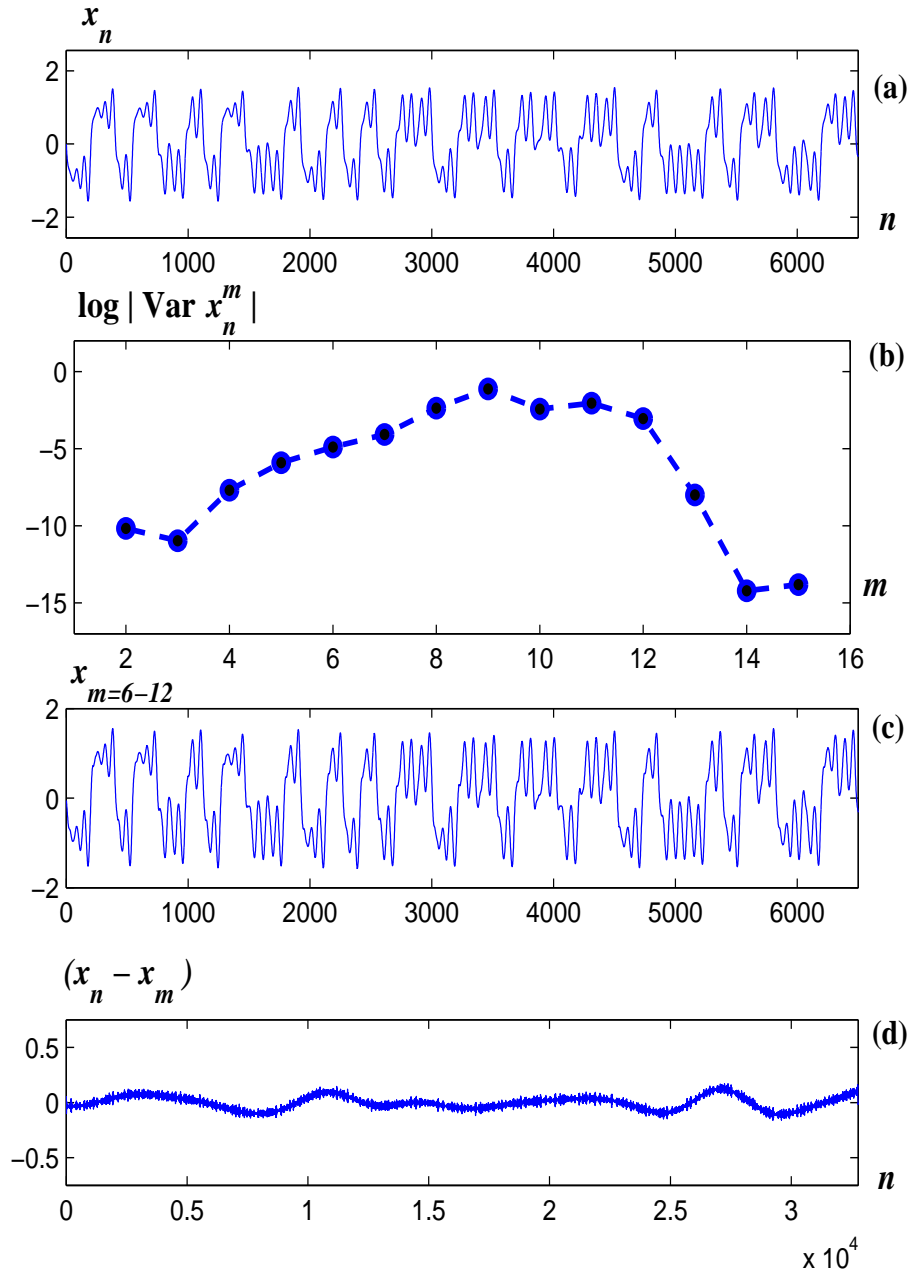
Figure 16: (Color online) The case $k = 0.3964$: (a) numerical time series of the $x$ state, (b) wavelet coefficient variance, (c) time series for the sum of the 6th to the 12th wavelet levels of the $x$ series, and (d) numerical errors between (a) and (c).